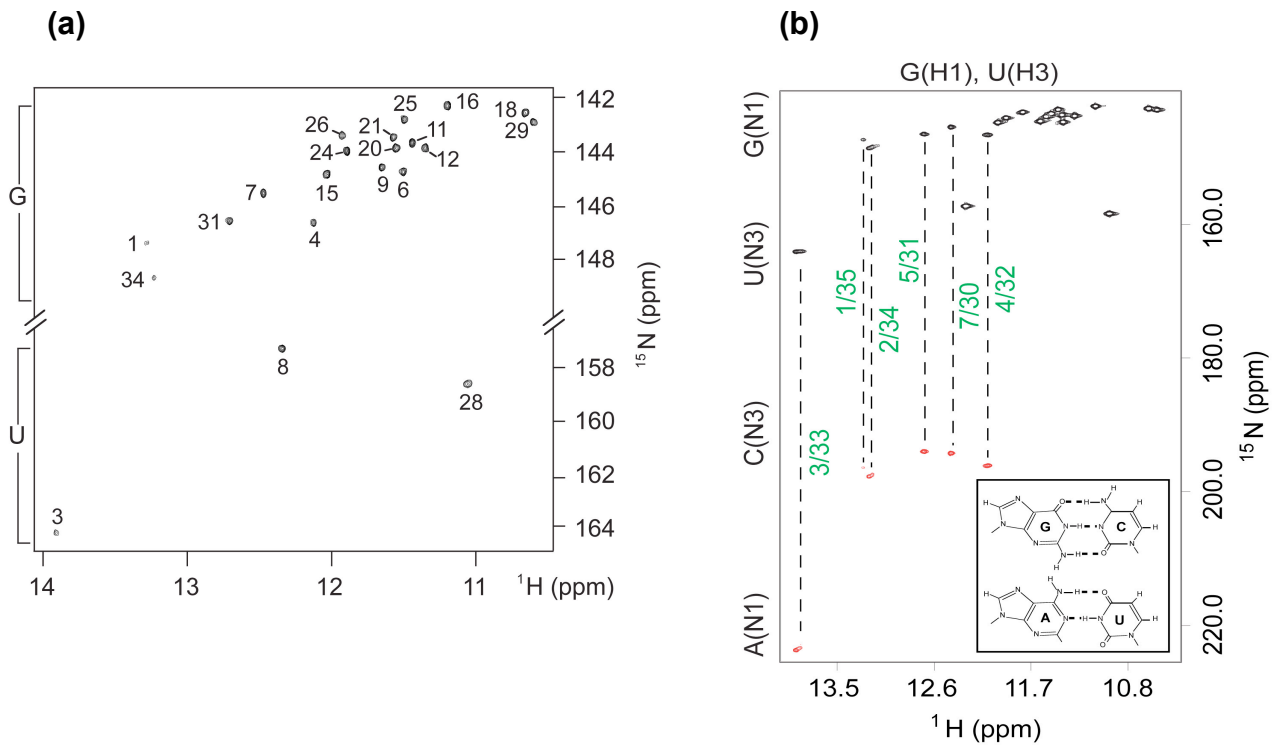

Supplementary Figure 1. **(a)** Through bond correlation of imino protons with attached nitrogens in the ^{1}H,^{15}N-HSQC spectrum of the RGG peptide - *sc1* RNA complex in 50 mM K-acetate, pH 6.8 at 25 ^{o}C. The cross peak assignments are based on known imino proton assignments established by site-specific labeling studies as shown in Fig. 2a.

(b) Through bond N-H••N correlation across Watson-Crick base pairs in the HNN-COSY spectrum of the RGG peptide - *sc1* RNA complex in 50 mM K-acetate, pH 6.8 at 25 ^{o}C. The cross peaks identifying N-H••N correlations across G•C and A•U Watson-Crick base pairs are labeled according to residue numbers. Insert shows base pairing alignments of Watson-Crick G•C and A•U base pairs with N-H••N hydrogen bonds.

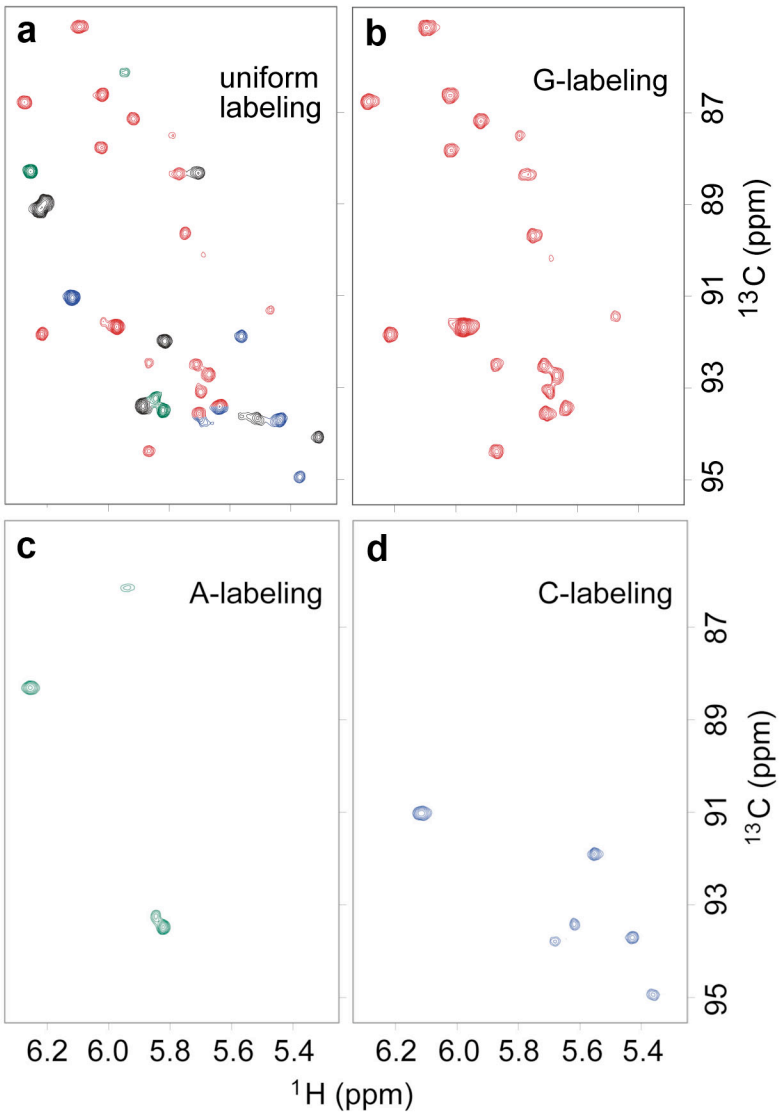

Supplementary Figure 2. Through bond correlation of C1'-H1' sugar atoms in the ^{1}H,^{13}C-HSQC spectrum of the RGG peptide - *sc1* RNA complex in 50 mM K-acetate, pH 6.8 at 25 ^{o}C. (**a**) Spectrum of the complex containing uniformly ^{13}C,^{15}N-labeled RNA. (**b**) Spectrum of the complex containing guanine-specific ^{13}C,^{15}N-labeled *sc1* RNA. (**c**) Spectrum of the complex containing adenine-specific ^{13}C,^{15}N-labeled *sc1* RNA. (**d**) Spectrum of the complex containing cytosine-specific ^{13}C,^{15}N-labeled *sc1* RNA.

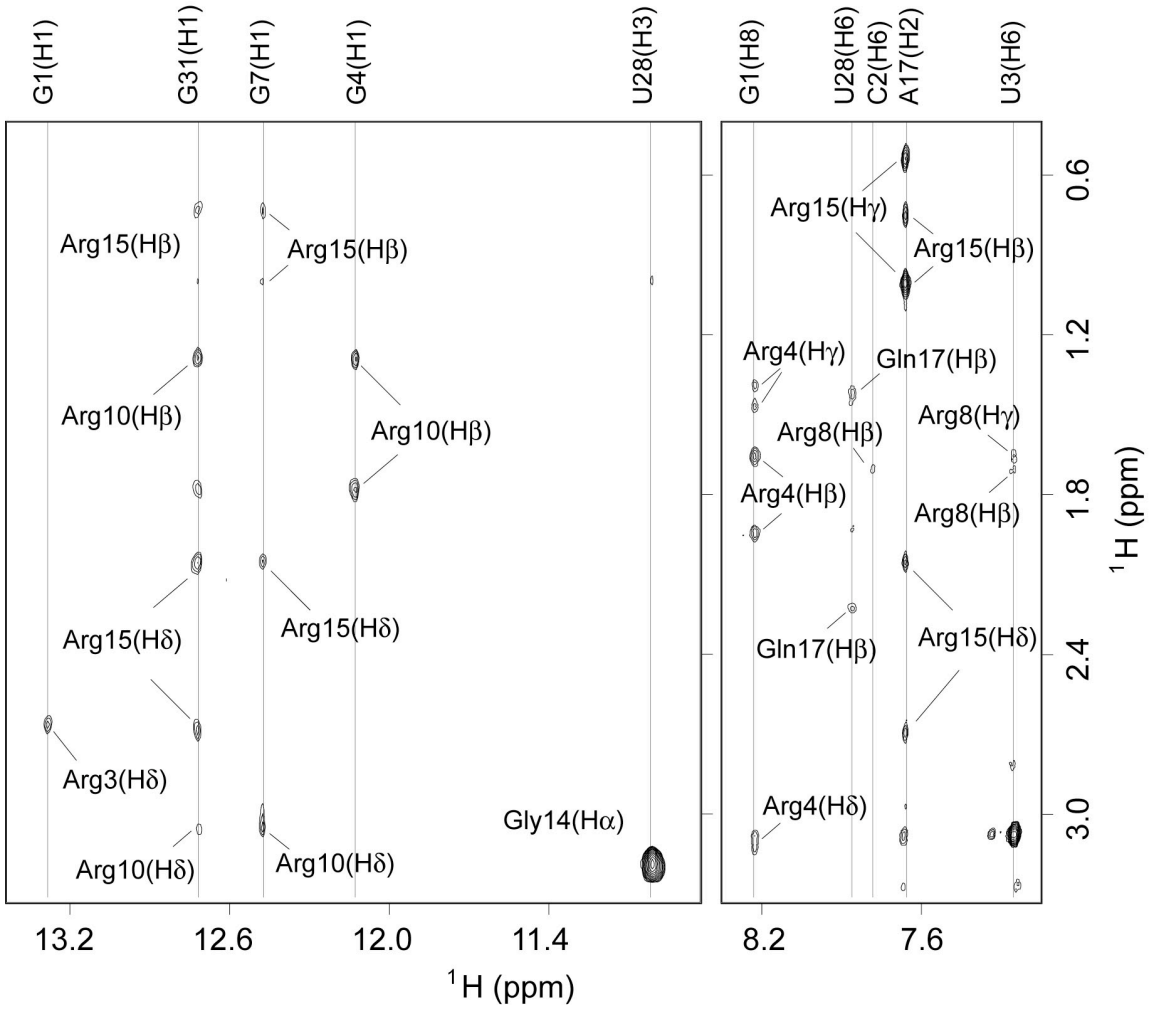

Supplementary Figure 3. Assignment of intermolecular peptide-RNA NOEs in the RGG peptide - *sc1* RNA complex. Identification of intermolecular ^{1}H-^{1}H NOEs in the NOESY spectrum of the complex.

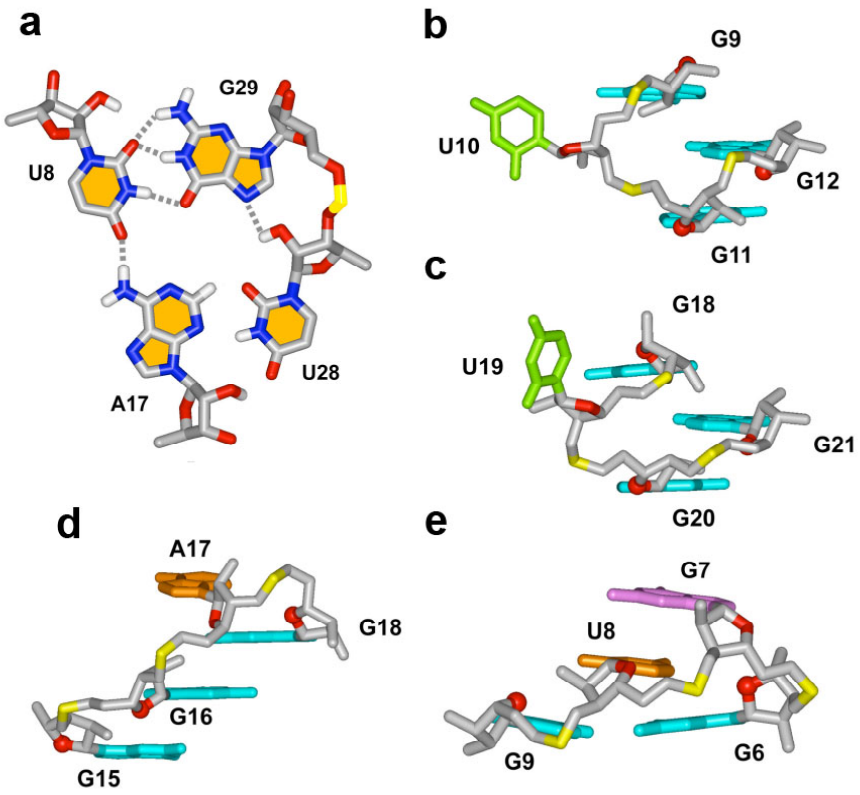

Supplementary Figure 4. (a) Proposed pairing alignment around the junctional U8•A17•U28•G29 tetrad in the solution structure of the RGG peptide - *sc1* RNA complex. The U8•G29 pair adopts a Wobble alignment in this arrangement.

Alignment of loop segments connecting G-tetrads within the G-quadruplex in the complex. (**b**) The single residue linker U10 connecting G9 and G11. (**c**) The single residue linker U19 connecting G18 and G20. In both panels (**b**) and (**c**) a single linker residue connects guanines with opposing strand orientations that are separated by a G-tetrad. (**d**) The single residue linker A17 connecting G16 and G18. (**e**) Linker G7-U8 connects G6 and G9 with similar orientations within the same G-tetrad.

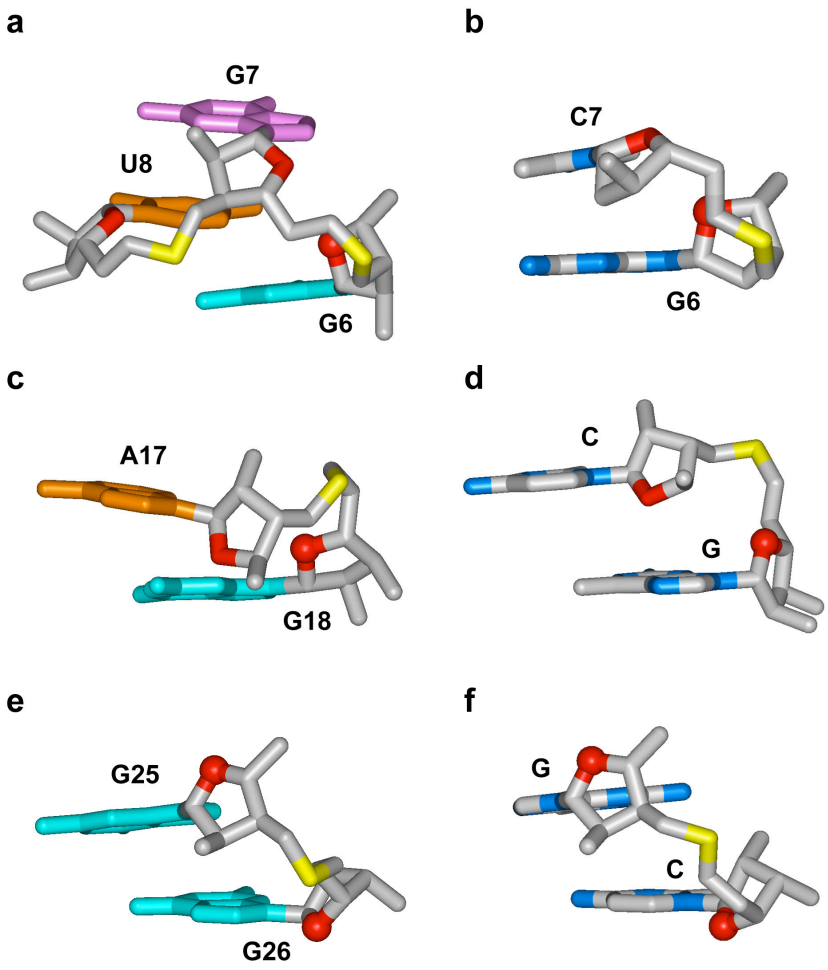

Supplementary Figure 5. Comparison of left-handed dinucleotide steps in bound *sc1* RNA with those reported for the streptomycin-binding RNA aptamer[59] and Z-RNA[60]. (**a**) Bottom-top left-handed G6-G7 step (with intercalation of U8) in bound *sc1* RNA and (**b**) G6-C7 step in streptomycin-binding RNA aptamer. Similar relative sugar orientations (O4´-to-O4´ contact) are observed for (**c**) the conformationally restricted A17-G18 left-handed step in bound *sc1* RNA and (**d**) the CpG step of Z-RNA. Similar relative sugar orientations (C3´-to-C3´ contact) are observed for (**e**) the G25-G26 left-handed step in bound *sc1* RNA and (**f**) the GpC step of Z-RNA.

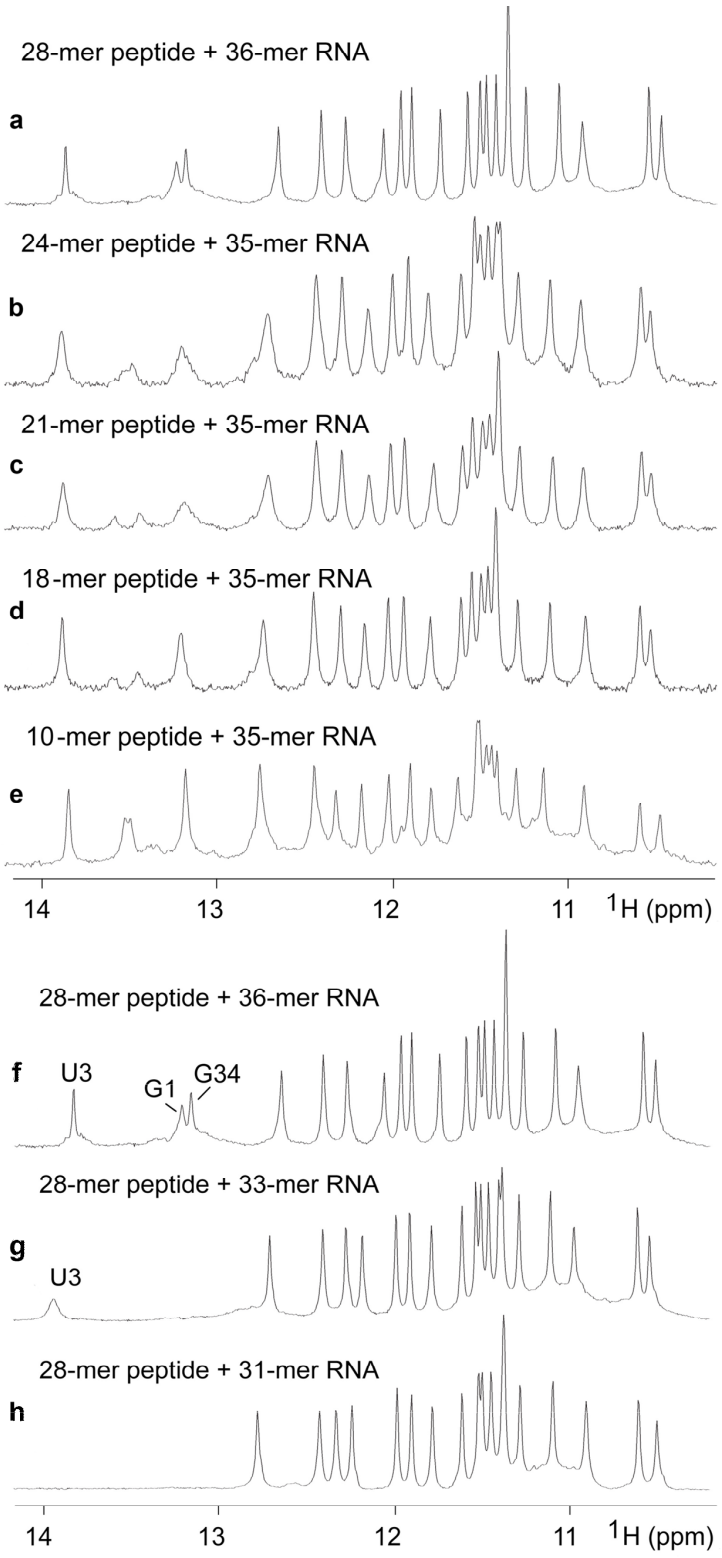

Supplementary Figure 6. (a-e) Imino proton NMR spectra of the RGG peptide - *sc1* RNA complex containing different lengths of bound RGG peptide. Complex

composed of 36-mer *sc1* RNA (G1 to G36) or 35-mer *sc1* RNA (G1 to C35) and (**a)** 28-mer RGG peptide (Gly1 to Gly28), (**b**) 24-mer RGG peptide (R3 to F26), (**c**) 21-mer RGG peptide (R3 to G23), (**d**) 18-mer RGG peptide (R3 to R20) and (**e**) 10-mer RGG peptide (R8 to Q17).

(f-h) Imino proton NMR spectra of the RGG peptide - *sc1* RNA complex containing different lengths of bound *sc1* RNA. Complex composed of 28-mer RGG peptide (Gly1 to Gly 28) and (**f**) 36-mer *sc1* RNA (G1 to G36), (**g**) 33-mer sc1 RNA (C2 to G34) and (**h**) 31-mer *sc1* RNA (U4 to A33).

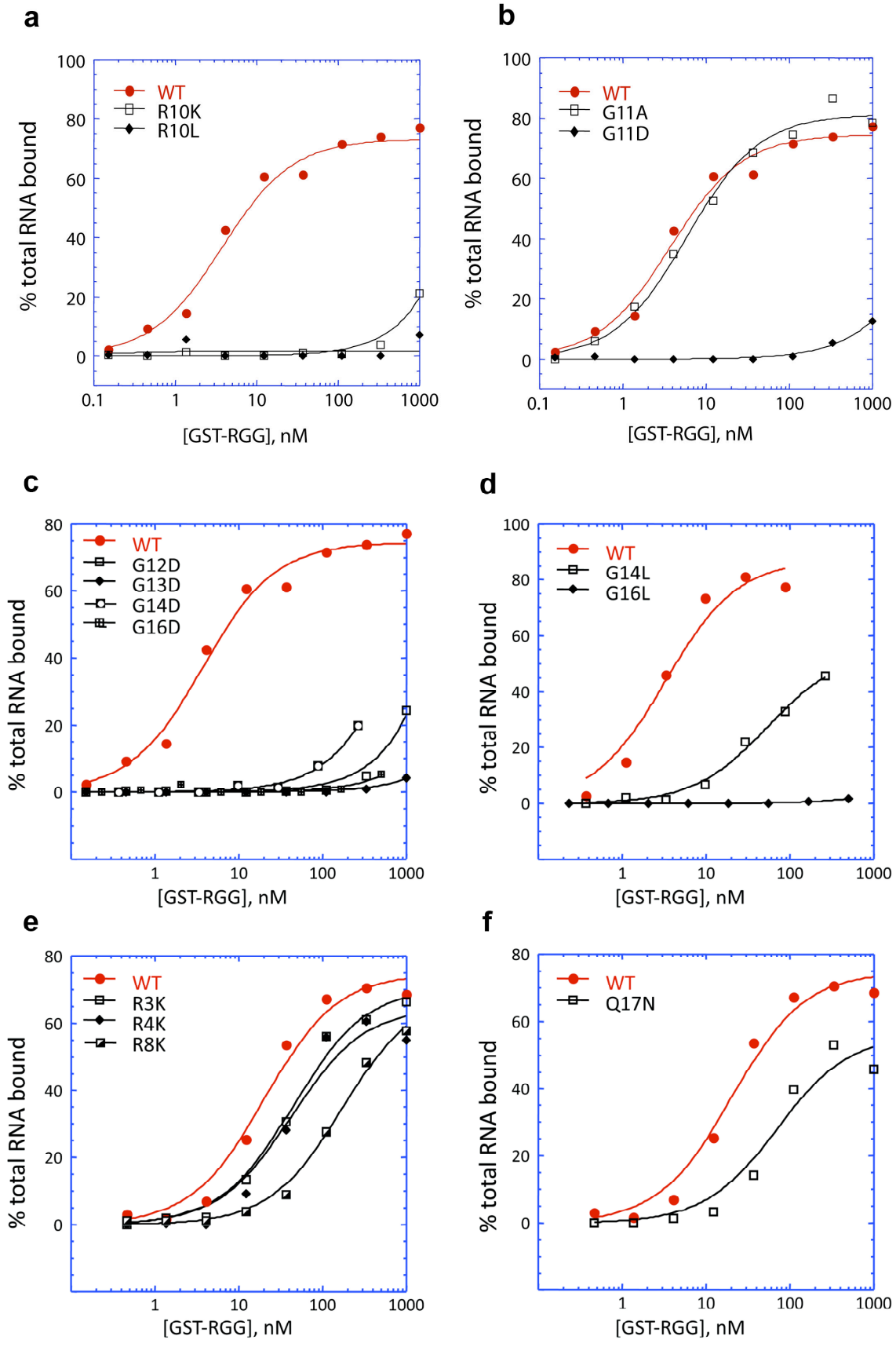
a
WT
R10K
R10L
% total RNA bound
[GST-RGG], nM
b
WT
G11A
G11D
% total RNA bound
[GST-RGG], nM
c
WT
G12D
G13D
G14D
G16D
% total RNA bound
[GST-RGG], nM
d
WT
G14L
G16L
% total RNA bound
[GST-RGG], nM
e
WT
R3K
R4K
R8K
% total RNA bound
[GST-RGG], nM
f
WT
Q17N
% total RNA bound
[GST-RGG], nM

Supplementary Figure 7. Assessment of the molecular determinants of the peptide for the FMRP RGG peptide - *sc1* RNA interaction by filter binding assay. (**a**) To assess the contribution of individual amino acids to *sc1* RNA binding affinity, mutations in the RGG box were evaluated. Mutation of Arg10 to Ala or Leu, abolished *sc1* RNA binding by the peptide. (**b**) Mutation of the glycines surrounding these crucial arginines. WT RGG (red circles, K_d = 3.8 nM), Gly11Ala (open squares, K_d = 5.9 nM), Gly11Asp (diamonds, K_d = ND). (**c**) Mutation of Gly12 (open squares), Gly13 (diamonds), Gly14 (half filled squares) and Gly16 (crossed squares) to Asp reduced binding by the FMRP RGG box by at least two orders of magnitude. WT RGG box (red circles) bound *sc1* with a Kd = 3.8 nM. (**d**) Mutation of Gly14 (open squares) to Leu, reduced peptide binding from Kd = 3.3 nM (WT, red circles) to 53.2 nM (black, open squares). The Gly16Leu mutation (diamonds) reduced binding to undetectable levels. (**e**) Mutation of other Arg residues in the RGG box reduced affinity for *sc1* somewhat (WT RGG (red circles, Kd = 20.3 nM), Arg3Lys (open squares, Kd = 45.3 nM), Arg4Lys (diamonds, Kd = 43.3 nM), Arg8Lys (half closed squares, Kd = 175 nM). (**f**) Mutation of Gln17 to Asn reduced the affinity of the FMRP RGG box (WT, red circles, Kd = 20.3 nM) by more than three-fold (Gln17Asn, open squares, Kd = 71.6 nM

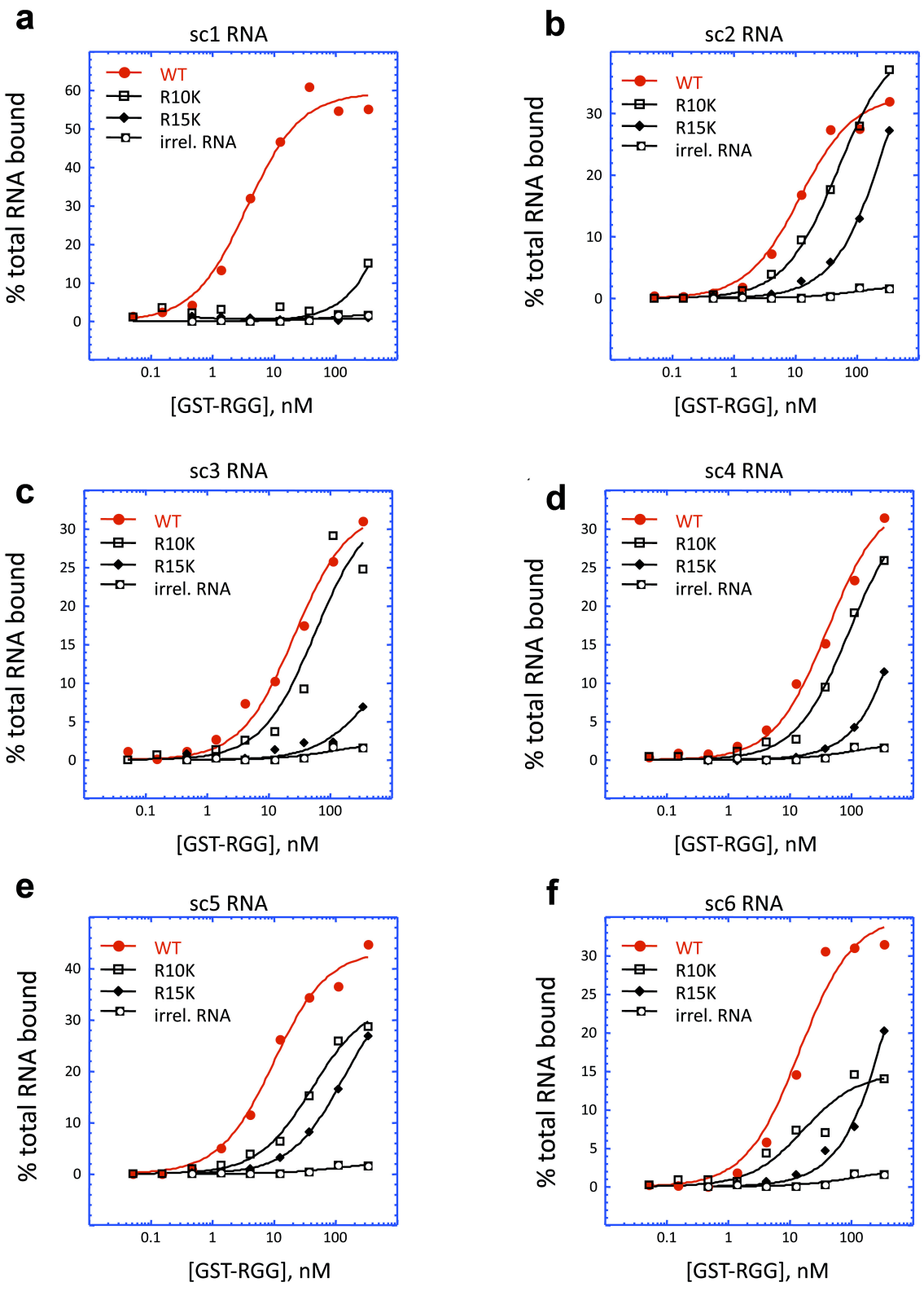

Supplementary Figure 8. Assessment of the affinity of the FMRP RGG box for *in vitro* selected RNA clones *sc1-sc6*. (**a-f**) The affinity of interaction of the

FMRP RGG box with full-length 96-mer RNAs was determined by filter binding assay using the indicated concentrations of purified GST-tagged wild-type (WT) RGG box (red circles) and two mutants, Arg10Lys (open black squares) and Arg15Lys (black diamonds). WT GST-RGG box was also tested for binding to an irrelevant *in vitro* selected RNA as a negative control (half filled black squares). Binding to the negative control was too low to determine a Kd. (**a**) *sc1* RNA: Kd for WT = 3.7 nM, Arg10Lys = ND, Arg15Lys = ND. (**b**) *sc2* RNA: Kd for WT = 12.1 nM, Arg10Lys = 49.5 nM, Arg15Lys = 345.1 nM. (**c**) *sc3* RNA: Kd for WT = 26.4 nM, Arg10Lys = 56.5 nM, Arg15KLys = 423 nM. (**d**) *sc4* RNA: Kd for WT = 40.7 nM, Arg10Lys = 91.3 nM, Arg15Lys = 2.16 uM. (**e**) *sc5* RNA: Kd for WT = 9.9 nM, Arg10Lys = 41.6 nM, Arg15Lys = 139 nM. (**f**) *sc6* RNA: Kd for WT =14.3 nM, Arg10Lys = 16.7 nM, Arg15Lys = 650 nM.

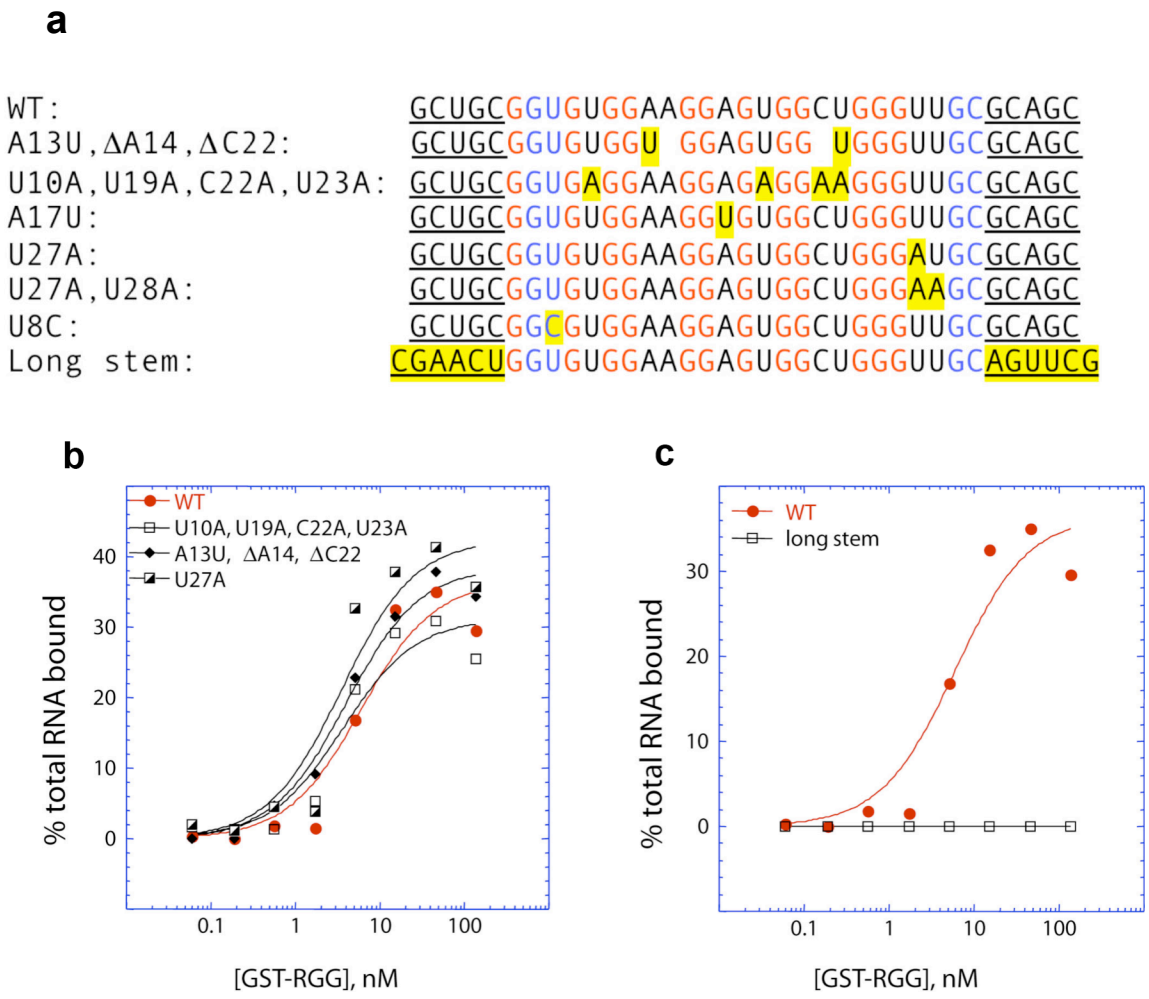

Supplementary Figure 9. (**a**) Sequence of *sc1* RNA mutants tested in panels **b** and **c**. WT (top line) is the wild-type 35-nt *sc1* RNA sequence obtained by *in vitro* RNA selection and deletion analysis. Deletions and mutations to this sequence are shown aligned to wild-type. Nucleotides forming the stem are underlined; guanines forming the G-tetrad core are shown in red; the last two base pairs of the stem are blue; modified residues are yellow.

The affinity of interaction of the FMRP RGG box with 35-mer *sc1* RNA (red) and mutations and deletions therein (black) was determined by filter binding assay using the indicated concentrations of purified GST-tagged wild-type (WT) RGG box and ^{32}P end-labeled commercially synthesized RNA (sequences listed in panel **a**). (**b**) Three of the tested RNAs with mutations in one-nucleotide and two-

nucleotide loops retained high affinity binding to the RGG box: K_d for WT = 6.0 nM (red circles), U27A = 3.6 nM (half closed squares), A13U,ΔA14,ΔC22 = 4.1 nM (diamonds), and U10A,U19A,C22A,U23A = 3.6 nM (open squares). (**c**) A longer and different stem resulted in a K_d too low to be measured by this assay.

Supplementary Table 1.

Chemical shift list of *sc1* RNA protons in the complex.

	Imino proton	Amino protons	H8/6	H2/5	H1'	H2'	H3'	H4'	H5'and H5''
G1	13.246		8.173		5.800	4.665	4.507	4.345	3.996; 3.690
C2		8.313; 6.803	7.729	5.562	5.624	4.362	4.254	4.334	4.550; 3.969
U3	13.868		7.200	4.507	5.444	4.247	4.298	4.371	4.339; 3.940
G4	12.082		7.617		5.647	3.990	4.375	4.306	4.441; 3.940
C5		8.870; 7.225	7.187	4.195	5.491	3.613	4.520	4.308	4.378; 4.065
G6	11.38	9.391; 6.994	7.503		5.973	5.200	4.885	4.256	4.444; 4.225
G7	12.430	7.998; 5.476	7.182		5.580	6.299	4.014	4.516	4.517; 3.545
U8	12.293		7.365	4.195	5.244	3.586	4.363	4.364	4.364; 4.155
G9	11.610	9.230; 6.225	7.435		5.958	4.512	4.921	4.580	4.586; 3.977
U10			7.936	6.006	6.146	4.546	4.791	4.470	4.704; 4.060
G11	11.382		7.822		5.640	4.795	4.632	4.370	4.513; 4.011
G12	11.281		7.211		6.232	4.318	4.841	4.572	4.500; 4.119
A13			8.481	8.218	6.191	4.862	4.876	4.626	4.292; 4.242
A14			8.114	7.257	5.760	4.624	4.619	4.417	4.470; 4.210
G15	11.984		7.584		5.414	4.128	4.385	4.367	4.365; 4.048
G16	11.093	9.167; 6.484	7.220		5.855	4.340	5.013	4.533	4.389; 4.050
A17			8.523	7.607	5.876	5.182	4.818	5.090	4.764; 4.106
G18	10.587	7.888; 4.872	7.265		5.730	4.620	4.413	4.609	4.471; 4.044
U19			7.988	5.998	6.161	4.526	4.878	4.509	4.566; 4.299
G20	11.538		7.926		5.681	4.778	4.707	4.400	4.211; 4.087
G21	11.496		7.789		6.048	4.790	4.860	4.563	4.321; 4.201
C22			7.962	6.128	6.058	4.370	4.721	4.569	4.437; 4.264
U23			7.734	5.697	5.731	4.340	4.582	4.434	4.216; 4.216
G24	11.922		7.928		5.626	4.504	4.375	4.382	4.274; 4.138
G25	11.446	8.443; 7.128	6.963		6.150	4.054	4.363	4.401	4.466; 4.412
G26	11.762	9.122; 5.921	7.959		5.717	4.303	4.935	4.671	4.241; 4.206
U27			7.831	5.866	5.824	4.414	4.773	4.582	4.468; 4.437
U28	10.964		7.805	5.939	5.633	4.017	4.641	3.996	4.554; 4.373
G29	10.519	6.410	7.380		5.810	5.186	4.365	4.323	4.139; 3.856
C30		8.594; 8.076	6.928	4.380	5.305	4.455	4.384	4.420	4.329; 4.088
G31	12.671		7.712		5.632	4.492	4.619	4.375	4.588; 3.979
C32		8.367; 6.962	7.650	5.145	5.374	4.536	4.466	4.360	4.573; 4.007
A33			7.726	6.385	5.781	4.392	4.551	4.398	4.439; 4.021
G34	13.190		7.164		5.602	4.241	4.395	4.328	4.464; 3.997
C35		8.501; 6.399	7.462	4.852	5.562	4.025	4.304	4.236	4.410; 3.932
G36			7.590		5.907	5.099	5.016	4.296	4.209; 4.088

Supplementary Table 2.

(a) Chemical shift list of RGG peptide protons in the complex.

	NH	Hα	Hβ	Hγ	Hδ	Hε	Hη/Hζ
G1		3.849					
P2		4.532	2.122; 2.018	1.903	3.562; 3.408		
R3	9.218	4.040	1.692; 1.219	1.510; 1.413	2.600	6.931	
R4	7.907	4.415	1.871; 1.600	1.402; 1.321	3.070; 3.030	7.520	
G5	8.537	3.888					
D6	8.020	4.662	2.858; 2.561				
G7	7.984	4.190; 3.529					
R8	8.669	3.937	1.641; 1.413	1.895; 1.608	3.011; 2.752	6.524	
R9	8.983	4.033	1.668; 1.656	1.590; 1.563	3.205; 3.175	7.164	
R10	7.181	4.543	1.727; 1.230	1.052; 0.656	3.022; 2.929	7.809	7.994; 6.820; 5.642
G11	8.171	4.022; 3.026					
G12	8.467	3.431; 3.209					
G13	8.644	3.857; 3.709					
G14	7.936	4.016; 3.133					
R15	7.185	3.791	0.937; 0.688	0.944; 0.479	2.630; 1.991	7.200	8.109
G16	8.952	4.155; 3.572					
Q17	8.060	4.462	2.167; 1.366	2.016; 1.877		6.950; 6.794	
G18	9.389	4.159; 3.742					
G19	8.636	3.997; 3.820					
R20	7.958	4.311	1.884; 1.716	1.510	3.133	7.246	
G21	8.456	3.883					
R22	8.253	4.297	1.843; 1.704	1.550	3.099	7.247	
G23	8.502	3.960					
G24	8.300	3.914					
G25	8.239	3.873					
F26	8.166	4.521	3.017		7.201	7.286	7.169
K27	8.227	4.232	1.760; 1.586	1.312	1.579	2.918	
G28	7.120	3.611; 3.555					

(b) Torsion angles in the R10-R15 peptide segment.

Residue	φ−torsion angle, deg	ψ−torsion angle, deg
R10	-66.1±5.1	144.7±7.9
G11	-68.4±4.3	-129.4±9.6
G12	58.0±5.5	-80.4±5.4
G13	-151.7±9.5	-169.2±6.9
G14	-38.8±1.8	-47.2±1.2
R15	-50.3±4.0	125.8±3.9

Supplementary Table 3.

Intermolecular cross-peaks in the FMRP RGG peptide - *sc1* RNA complex.

Residue		P2	R3			R4				G7	R8				R10			G11	G12		G13		G14		R15					Q17	
proton		β	h	δ	γ	α	β	δ	γ	α	h	β	δ	γ	β	δ	γ	h	h	α	h	α	h	α	h	α	β	γ	δ	β	γ
G1	H1			●																											
	H8					●	●	●	●	●																					
	H3′										●																				
	H5′												●																		
C2	H5										●	●	●	●																	
	H6										●	●	●	●																	
	41	●																													
	42	●									●																				
U3	H3														●			●													
	H5											●	●	●																	
	H6											●	●	●																	
G4	H1														●																
	H8																		●	●											
C5	H5																	●	●	●											
	H6																		●	●											
	41														●	●	●	●										●	●	●		
	42														●	●		●										●		●		
G7	H1															●												●		●		
A17	H2																										●	●	●	●		
	H8																				●										
	H1′																				●	●	●								
G18	H1																											●			
U28	H3																						●		●						
	H5																													●	●
	H6																													●	●
	H1′																										●	●	●	●	●
	H2′																													●	
C30	41															●															
	42																●														
G31	H1														●	●												●		●		
C32	41														●		●														
	42														●																
C35	41		●		●																										
	42		●		●																										

SUPPLEMENTARY TEXT

Guanine imino protons that exhibit slow exchange in the complex

The structure of the RGG peptide - *sc1* RNA complex contains four tetrad planes with the mixed U8•A17•U28•G29 and G11•G15•G20•G24 tetrads sandwiching the G9•G26•G18•G6 and G12•G16•G21•G25 tetrads (**Figs. 5e,f**). In such an arrangement, the prediction would be that the imino protons of the sandwiched G-tetrads would exhibit the slowest hydrogen exchange[33]. Indeed, hydrogen exchange data establish that the slowest exchanging imino protons are G9, G26, G18 and G6 that are associated with the G9•G26•G18•G6 and G12, G16, G21 and G25 that are associated with the G12•G16•G21•G25 tetrad (**Fig. 1f**).

Shape complementarity contributes to peptide-RNA recognition

The structure of the complex nicely explains the requirement for an RGG peptide for targeting the *sc1* RNA. The bound peptide and the walls of the RNA pocket interact through shape complementarity, given that filter-binding assays establish that there is an absolute steric requirement for two glycines (Gly12 and Gly13) and a less stringent requirement for two other glycines (Gly11 and Gly14) positioned between Arg10 and Arg15 for complex formation (**Fig. 7b and Supplementary Fig. 7b, d**). The four Gly residues facilitate the reverse turn (ϕ, φ values for the $R_{10}GGGGR_{15}$ segment are listed in **Supplementary Table 2b**) that position the side chains of Arg10 and Arg15 for targeting the RNA scaffold. The dimensions of the pocket are such that any side chain at positions 12 (clashes with C5 and Arg15 side chain) and 13 (clashes with A17 and Arg15 side chain) would result in spatial clashes with the walls of the pocket, while there is more room to accommodate a side chain at position 14, given that the latter position is directed outwards from the pocket. Incorporation of a side chain at position 11 could potentially spatially clash with atoms of U3 and G4, and could also disrupt the Gly11(NH)-G4(N7) hydrogen bond in the complex.

Arginine•guanine pairing contributes to peptide-RNA recognition

In addition to peptide-RNA steric complementarity, the specificity of FMRP RGG peptide - *sc1* RNA recognition is dictated by a pair of arginine•guanine intermolecular hydrogen-bonding contacts within the complex. The reverse turn adopted by the $R_{10}GGGGR_{15}$ RGG peptide segment orients the side chains of Arg10 and R15 in opposing directions and displaced relative to each other, such that they are ideally positioned to interact with the major groove edges of adjacent guanines G31 and G7 on partner strands (**Figs. 6c,d**). Indeed, the importance of the Arg15•G7 and Arg10•G31 interactions are highlighted from mutation studies, which establish that mutation of either Arg10 (**Supplementary Fig. 7a**) or Arg 15 (**Fig. 7a**) on the one hand, or modification of the major groove edges of G7 and G31 through deaza modifications (**Fig. 7d**) on the other, results in dramatic loss of binding affinity, as measured by filter-binding assays. Such arginine•guanine pairing alignments are a recurring theme in protein-RNA recognition[29], but the cross-brace interaction reported in this study appears to be novel and specific to the FMRP RGG peptide - *sc1* RNA complex.

Significance of binding to duplex-quadruplex junction in determination of FMRP target RNAs

The Fragile X mental retardation protein, FMRP, is one such RNABP whose loss-of-function leads to devastating effects on human cognition. This polyribosome-associated protein is believed to regulate the translation of proteins whose activity-dependent synthesis at synapses underlies many forms of synaptic plasticity. The I304N mutation, in human and mice, highlights the significance of RNA binding to Fragile X Syndrome[16]. The significance of the RGG box - G-quadruplex interaction is underscored by the observation that among the three *Fmr1* paralogs, only FMRP is able to bind to G-quadruplexes[17].

The bioinformatic prediction of genomic quadruplex motifs suggests widespread impacts on biology, but paradoxically complicates the identification of the key RNAs harboring this motif that are targeted by RNA regulatory proteins and pathways. The current study suggests that in the case of FMRP-RNA target studies, efforts to identify G-quadruplexes alone may be insufficient for

discriminating true targets, as the importance of interactions with guanines at the junction of the G-quadruplex and duplex play a key, but unexpected role, in FMRP-RNA interactions. This may underlie the limited (~50%) extent to which FMRP candidate target RNAs harboring G-quadruplexes have been biologically validated[12].

SUPPLEMENTARY METHODS

Structure calculations details. We outline below details of the structure calculations that were not included in the Online Methods section due to space limitations.

Step 1: In the heating stage, the regularized extended RNA chain was subjected to 60 ps of torsion-angle molecular dynamics at 20,000 ^{o}K using a hybrid energy function composed of geometric and NOE terms. The van der Waals (vdW) component of the geometric term was set to 0.1, thus facilitating torsional bond rotations, while the NOE term included NOE-derived distances with the scaling factor of 150. The structures were then slowly cooled from 20,000 ^{o}K to 1,000 ^{o}K over period of 60 ps during which the vdW term was linearly increased from 0.1 to 1. At the third stage, molecules were slowly cooled from 1000 ^{o}K to 300 ^{o}K for 6 ps of Cartesian molecular dynamics[55].

Step 2: A pre-folded quadruplex RNA molecule with an unstructured duplex stem part was used as a starting fold for 10 separate attempts of torsion dynamics computations. The set of active restraints at this stage included all RNA duplex restraints listed in Table 1. For the quadruplex component, only hydrogen-bonding and χ torsion restraints were active during this stage. Torsion dynamics protocol was similar to that described for quadruplex fold except that temperature in the heating stage was set to 40,000 ^{o}K. Eight out of ten structures with minimal energies were selected and subjected to Cartesian dynamics calculations as described earlier[55], with all restraints in the RNA part switched on during the computations.

At step 3, the temperature at the heating stage was set to 50,000 ^{o}K. A total of 100 combined molecules were generated, of which the top 20 structures

with minimal energies and no NOE > 0.5 Å violations were subjected to restrained molecular dynamics with activated torsion restraints for peptide and RNA. Of these, 15 molecules were selected based on minimal energy, minimal vdW energy term and minimal number of violations.

At step 4, the results of conformational analysis of R10 and R15 side chains were taken into account, as follows. There are 8 possible configurations of the arginine side chain hydrogen-bonded with the Hoogsteen edge of a guanine base through two hydrogen bonds. Each of these configurations enforced by hydrogen bonds was examined for R10 and R15 side chains during de-novo distance-restrained folding of the peptide-RNA complex. From the pool of initially obtained molecules, a selected minimal energy complex of each variant was subsequently refined by Cartesian dynamics and minimization, with added planarity restraints on guanine base and argininamide group. Out of 8 configurations for each residue (R10 and R15) only 3 were selected after inspection and calculation of Ramachandran plots as stereochemically feasible in the final complexes. Furthermore, experimentally observed restraints between the epsilon proton of R10 and H8 proton of G31, and between two eta protons of R15 and H8 of G7 served to select a single conformation out of the three obtained computationally. The resulting conformations for R10/G31 and R15/G7 were enforced by hydrogen bonds and planarity restraints during computations of ten molecules shown on Fig. 4a. The conformation of R10 is shifted, implying that eta protons of R10 are likely to be engaged in hydrogen bond formation with phosphate group of RNA or neighboring peptide atoms.

Step 5: After solvation and introduction of cations, the water-cation shell was equilibrated for 20 psec of molecular dynamics with time step set to 1 fsec. Coordinates of RNA-peptide complex atoms were fixed at this stage. At the next step, experimental distance and torsion restraints were imposed on RNA-peptide and the full system, with release of the fixed coordinates of RNA-peptide, was subjected to energy minimization. The computations were carried out with a distance-dependent dielectric constant ($\varepsilon = 4r$, where r stands for the distance between two atoms) with convergence criteria having root mean square gradient

less than 0.1 kcal mol^{-1} $Å^{-2}$. After initial minimization, 10 psec of distance-restrained molecular dynamics computations at 300 ^{o}K with 1 fsec time step were carried out on fully solvated complex, followed by final energy minimizations.

In order to improve convergency of the resultant ensemble of 10 molecules, additional minimization was performed with X-PLOR-NIH program, which allowed addition of soft planarity restraints on G-tetrads and base pairs (3 kcal mol^{-1} $Å^{-2}$). To preserve the geometry of the hydrated complex calculated with AMBER force-field parameters at the preceding stage, the sugar-phosphate torsion angles were measured in hydrated structures, and they were used as restraints in final short minimization round of 1000 steps with X-PLOR-NIH. Backbone torsion angles in the peptide part were improved after Ramachandran plot analysis by enforcing closest favorable set of ϕ/ψ angles for non-Gly amino-acids (procedure affecting from 0 to 3 residues in the ensemble of 10 molecules).

The groove size and helical axis of the bound *sc1* RNA in the complex was calculated using the CURVES program[56].

***In vitro* RNA transcription for filter binding assays.** Wild-type and mutant *sc1* RNA were prepared by *in vitro* transcription in the presence of alpha-^{32}P-UTP from DNA templates produced by PCR exactly as previously described[17]. Briefly, transcribed RNA was purified by 8% urea-PAGE, phenol-chloroform extracted, precipitated, and resuspended in RNAse-free water, as described, and adjusted to 1,000 cpm/ul in 1X SBB buffer (200 mM KOAc, 50 mM TrisOAc at pH 7.7, 5 mM MgOAc) for filter binding assay.

Cloning, expression and purification of GST-fusion proteins. Complementary synthetic DNA oligonucleotides were designed to alter the human FMRP RGG box in its codon usage to match that of *E. coli* without changing the human amino acid sequence (5'GGATCCCGCCGCGGTGATGGTCGTCGTCGTGGTGGTGGCGGCCGCGGT CAGGGTGGCCGCGGTCGTGGTGGCGGCTTTAAAGGTTAAGAATTC-3'

encoding RRGDGRRRGGGGRGQGGRGRGGGFKG) and cloned into the BamHI and EcoRI sites of pGEX-6P to generate N-terminally GST-tagged RGG box fusion proteins. These were expressed by IPTG induction (1 mM, 3 hours) in BL21(DE3)Star cells (Invitrogen) and purified on Glutathione Fast Flow 4 Sepharose columns (GE Life Sciences), washed with 1X PBS, 1 mM EDTA, 1 mM DTT buffer and eluted with 50 mM reduced glutathione in 50 mM Tris, pH 8.0, 100 mM NaCl, 0.1% Triton X-100, 1 mM DTT buffer by conventional methods. Mutations to this sequence were introduced using the Stratagene QuikChange Site-directed mutagenesis kit (Agilent) and confirmed by sequencing of both DNA strands from positive clones. Purity of the fusion proteins was assessed by 14% SDS-PAGE gel analysis after staining with GelCode blue (Pierce). Proteins were used for filter binding assays without cleavage of the GST moiety to increase binding of the otherwise small peptides to the nitrocellulose filter.